CHEMISTRY OF MATERIALS

Article

Cite This: Chem. Mater. 2019, 31, 8394−8401

pubs.acs.org/cm

Memristive Electronic Synapses Made by Anodic Oxidation

Shaochuan Chen,[†,‡] Seyedreza Noori,[∥] Marco A. Villena,[†,⊥] Yuanyuan Shi,[#] Tingting Han,[†] Ying Zuo,[†] MariaPia Pedeferri,[∥] Dmitri Strukov,[‡] Mario Lanza,[*,†] and Maria Vittoria Diamanti[∥]

[†]Institute of Functional Nano and Soft Materials, Collaborative Innovation Center of Suzhou Nanoscience & Technology, Soochow University, Suzhou 215123, China

[‡]Department of Electrical and Computer Engineering, University of California at Santa Barbara, Santa Barbara, California 93106−9560, United States

[∥]Department of Chemistry, Materials and Chemical Engineering "G. Natta", Politecnico di Milano, Via Mancinelli 7, Milan 20131, Italy

[⊥]Department of Electrical Engineering, Stanford University, Stanford, California 94305, United States

[#]Andrew and Erna Viterbi Faculty of Electrical Engineering, Technion—Israel Institute of Technology, Haifa 32000, Israel

Supporting Information

Downloaded via UNIV OF CALIFORNIA SANTA BARBARA on January 14, 2021 at 20:35:26 (UTC).
See https://pubs.acs.org/sharingguidelines for options on how to legitimately share published articles.

ABSTRACT: Memristors have recently gained growing interest due to their potential application as electronic synapses to build artificial neural networks for artificial intelligence systems. However, modulating the conductivity of memristors in a dynamic way to emulate biological synaptic behaviors is very challenging. Here we show the first fabrication of memristive electronic synapses using a dielectric film (TiO_{2-x}) synthesized via an electrochemical anodization method. Pt/anodic TiO_{2-x}/Ti memristive synapses show reliable and reproducible memristive behavior and fast switching times below 90 ns. By applying ramped voltage stresses, multilevel conductance states have been achieved (using different current compliances or reset voltages), and by applying pulsed voltage stresses, the potentiation and depression rates could be accurately controlled by tuning the pulse amplitudes. The switching is governed by homogeneous charge rearrangements at the TiO_{2-x}/Ti interface and TiO_{2-x} thickness modulation. It is concluded that the anodic oxidation method may be a cheap and effective route to fabricate competitive electronic synapses.

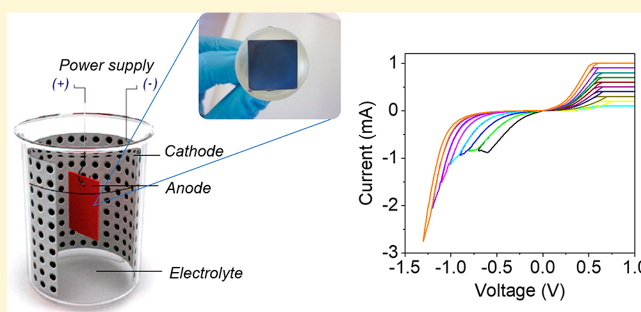

■ INTRODUCTION

Conventional von Neumann computing architectures implemented via complementary metal−oxide−semiconductor (CMOS) integrated circuits have encountered bottlenecks in terms of speed and energy efficiency, and thus, they are hardly adequate for meeting the demands for processing the vast and growing amounts of data required by modern societies.[1−3] Recent studies have shown that the inherent limitations of conventional CMOS-based computing architectures could be overcome via hardware implementation of bioinspired neuromorphic computation systems.[4] In such systems, electronic devices are designed to emulate biological synaptic functions, which in turn results in efficient implementation of many cognitive tasks, such as perception and learning.[5−7] In biological synapses, the key elements of such an approach are cellular membranes that connect a preneuron and a postneuron and that allow electrical stimuli transmission from one to another after different time intervals by modulating their conductivity dynamically, thanks to the segregation of Ca^+ and Na^+ ions.[3] Emulating this plastic connection strength using electronic devices is very challenging, and despite bioinspired neural networks having been constructed using phase change memories,[2] ferroelectric junctions,[8] and transistors,[9] the race to find electronic devices with superior ability to emulate synaptic functions remains open.

The fabrication of artificial synapses for neuromorphic systems using memristors has recently attracted significant attention due to their capability to emulate synaptic plasticity.[10−15] Memristors are two-terminal metal/insulator/metal (MIM) cells that can show resistive switching (RS); i.e., the conductance of the insulator can be intentionally tuned to reach different stable resistive states when specific external electrical stimuli are applied between the two metal electrodes.[16−20] The easy fabrication and excellent three-dimensional integration capability of memristors are immediate advantages compared to CMOS transistors.

The main desired features for memristors in artificial neural networks are multilevel conductance states, stable and gradual

Received: June 8, 2019
Revised: September 19, 2019
Published: September 20, 2019

© 2019 American Chemical Society

DOI: 10.1021/acs.chemmater.9b02245
Chem. Mater. 2019, 31, 8394−8401

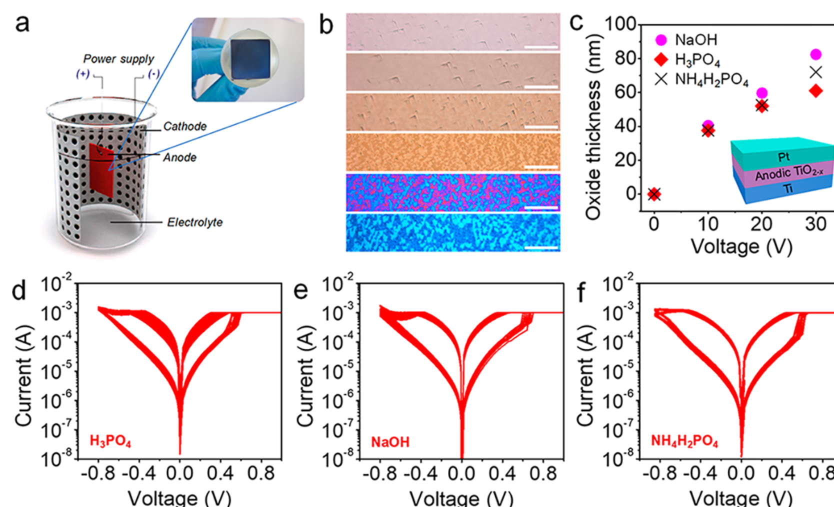

Figure 1. Fabrication of anodic memristive synapses. (a) Schematic of the electrochemical growth of TiO_{2-x} films on Ti substrates. (b) From top to bottom: optical microscope images of anodic TiO_{2-x} films created by using H_3PO_4 as anodizing electrolyte at 2.5, 5, 7.5, 10, 20, and 30 V bias, respectively. Typical color indicates the different thicknesses of the anodic titanium oxide films, which are 10, 17, 20, 35, 50, and 65 nm. The scale bars are 200 nm in all images. (c) Oxide thickness vs anodizing voltage in the three electrolytes considered; the thickness is calculated from spectrophotometric measurements, and the inset shows the structure of the fabricated Pt/anodic TiO_{2-x}/Ti memristors. (d) $I-V$ curves collected in Pt/10 nm TiO_{2-x}/Ti devices in which the TiO_{2-x} films have been anodized at 2.5 V using H_3PO_4, (e) NaOH, and (f) $NH_4H_2PO_4$ as electrolytes. Only 50 cycles were shown in each device for clarity. All the devices show stable set and reset transitions.

potentiation and depression dynamics,[3,4,14] and low operating voltage.[21] Despite the great progress experienced in the last few years, memristors are still unable to fulfill all these technological requirements, which is delaying their final implementation in neuromorphic systems. Therefore, finding new materials combinations and synthesis methods to produce MIM-based memristors with optimal performances is necessary. Here we present the first use of an electrochemical technique (anodic oxidation) to synthesize TMO dielectrics for memristive electronic synapses. The devices exhibit excellent synaptic plasticity, i.e., progressive potentiation and depression that can be accurately controlled via voltage, fast response time down to 100 ns, low cycle-to-cycle variability, and excellent stability of the set and reset voltages at high temperature. Despite the synthesis of TMO films using anodic oxidation being known for years,[22] we are not aware of any report using this method to fabricate memristive electronic synapses. The only report in this direction can be found in ref 23, in which the authors fabricated memristive $Pt/Ta_2O_5/Ta$ cells with sizes ranging from 25 μm × 25 μm to 100 μm × 100 μm for nonvolatile information storage. However, the synaptic response of memristors fabricated via an electrochemical anodization method has never been explored before.

■ RESULTS AND DISCUSSION

Figure 1a illustrates the schematic of electrochemical growth of TiO_{2-x} films. Titanium substrates of commercial purity (99.2%) and 2.0 mm thickness were purchased by Alfa Aesar. The substrates were cut into pieces of 2 cm × 2 cm and were mechanical polished using abrasive paper (starting from 600 to 4000 grit), followed by 0.3 μm alumina suspension for final polishing until a near mirrorlike surface was achieved. The oxidation of Ti substrates was carried out by connecting them to the positive pole of a direct current (DC) power supply, while the negative pole was connected to a stainless steel needle attached to a syringe containing the electrolyte (see Figure 1a). Three different electrolytes have been used: H_3PO_4 (phosphoric acid, 0.5 M), NaOH (sodium hydroxide, 0.5 M), and $NH_4H_2PO_4$ (ammonium dihydrogen phosphate, 0.5 M). The anodic oxidation processes have been conducted potentiostatically by applying constant voltage,[24] which we will call here anodization voltage (V_A), and it was maintained for 15 s. For each electrolyte, different V_A values ranging from 2.5 to 30 V have been used. The application of bias produced the oxidation of the Ti substrates into Ti^{4+}, and then the Ti^{4+} cations react with O^{2-} from the electrolytes, producing TiO_{2-x} films on the surface of the Ti substrate. This process follows the electrochemical reactions described in eqs 1−3.

$$Ti \rightleftharpoons Ti^{4+} + 4e^- \quad (1)$$

$$H_2O \rightleftharpoons 2H^+ + O^{2-} \quad (2)$$

$$Ti^{4+} + 2O^{2-} \rightleftharpoons TiO_2 \quad (3)$$

Yet, the complex nature of the electrochemical process generally ensures the formation of a nonstoichiometric oxide, with formula TiO_{2-x}, rather than of pure TiO_2. The thickness, morphology, and structure of the anodic TiO_{2-x} films can be controlled by tuning the anodizing parameters (see the Methods), i.e., V_A, electrolytic solution, electrolyte concentration, and composition of the metal substrate.[22,25] The anodic oxidation processes have been carried out in three electrolyte chambers under different anodizing voltages (V_A). After the electrochemical anodization step, the surface of the samples was rinsed, cleaned with deionized water, and dried with a compressed air gun. Figure 1b shows the optical microscope images of TiO_{2-x} films anodized using 0.5 M H_3PO_4 electrolyte at V_A values of 2.5, 5, 7.5, 10, 20, and 30 V, which resulted in TiO_{2-x} films with thicknesses ranging over 10, 17, 20, 35, 50, and 65 nm (respectively), as estimated by spectrophotometry (see the Methods); in the other electrolytes, similar results were found, with a slight difference in the anodizing ratio—the relationship between voltage applied and thickness obtained—in the case of NaOH, where oxides showed a slightly higher thickness (Figure 1c).[26] For thin

DOI: 10.1021/acs.chemmater.9b02245
Chem. Mater. 2019, 31, 8394−8401

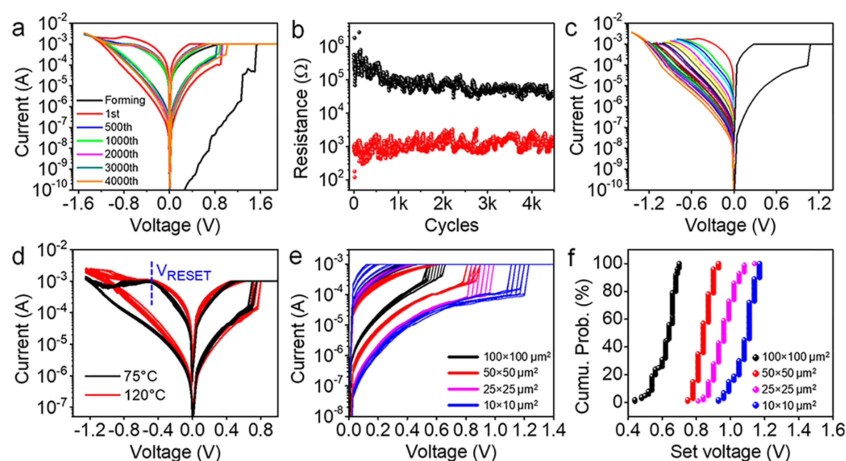

Figure 2. Figures of merit for anodic memristive synapses. (a) $I-V$ curves collected on a Pt/10 nm TiO_{2-x}/Ti device (V_A = 2.5 V, NaOH) showing very low cycle-to-cycle variability for more than 4500 $I-V$ cycles. (b) Corresponding resistance vs cycle plot showing that the LRS/HRS ratio is near 100; the HRS and LRS currents are read at 0.1 V in each cycle. (c) Progressive reset process of Pt/TiO_{2-x}/Ti memristive devices. (d) Extracted 10 cycles collected in a Pt/10 nm TiO_{2-x}/Ti device at 75 °C (first) and 120 °C (last); the set and reset processes show no temperature dependence. (e) Representative set curves of Pt/10 nm TiO_{2-x}/Ti devices (2.5 V, NaOH) with sizes ranging from 100 μm × 100 μm to 10 μm × 10 μm; the smaller devices show higher initial resistance and higher set voltages. (f) Corresponding cumulative probability distribution of the set voltages of devices analyzed in part e. One hundred data points have been collected for each device size.

anodic TiO_{2-x} films (V_A up to 10 V), the thickness can be calculated by Faraday's law using the total charge in the anodization system (see the Methods). It should be noted that under high anodizing voltages (V_A is higher than 10 V in this study), a relevant parasitic process (O_2 evolution) may occur subtracting current from the oxide growth. Partial crystallization may take place at the TiO_{2-x}/Ti interface, changing amorphous TiO_{2-x} film to partially polycrystalline,[27] thus causing higher thickness fluctuation under the same electrolytes. The color of the TiO_{2-x} surface changes with the film thickness. The topographic maps collected via atomic force microscopy (AFM) indicate that the root-mean-square (RMS) roughness of the surface of the 10 nm TiO_{2-x}/Ti samples is <1.1 nm [see Supplementary Figure S1, Supporting Information (SI)]. This value is larger than that of TiO_{2-x} samples grown by atomic layer deposition (ALD), typically 0.2 nm,[28] but it is still suitable for the fabrication of MIM-like memristors. For example, in ref 29 memristors with a very high endurance of 10^{12} cycles were fabricated using Ta_2O_{5-x}/TaO_{2-x} film with a much larger RMS surface roughness. In fact, the RMS roughness of the TiO_{2-x}/Ti sample may be related to the roughness of the polished Ti substrate, not to thickness fluctuations within the TiO_{2-x} film. The $I-V$ curves collected via conductive AFM (see Supplementary Figure S1d, SI) show low dispersion of the onset potential (V_{ON}), which is defined as the minimum voltage at which current above the noise level (~1 pA) can be detected; this indicates that the thickness and composition of the TiO_{2-x} film are reasonably homogeneous—or at least that, from an electrical point of view, it is as homogeneous as other high-k dielectrics deposited via ALD and/or sputtering.[30,31] A thicker anodic TiO_{2-x} device can exhibit larger onset potential (see Supplementary Figure S1e, SI). This experiment was repeated for the growth of oxides in H_3PO_4 electrolyte under V_A = 2.5, 5, and 7.5 V (see Supplementary Figure S2, SI), which confirmed the good electrical homogeneity of the anodic TiO_{2-x} films. The electrical homogeneity of the anodic films has been further confirmed by the CAFM current map (Supplementary Figure S3, SI). Avoiding large V_{ON} fluctuations at different locations on the sample is important to reduce device-to-device variability, which is critical in memristive technologies.[17,32]

After the growth of TiO_{2-x}, top Pt electrodes are deposited on the TiO_{2-x} layer to fabricate MIM structure memristors (see the inset in Figure 1c). The use of vertical memristors to fabricate electronic synapses is an immediate advantage compared to all previous reports using planar memristors,[33,34] as these occupy larger areas and cannot be stacked vertically. Parts d, e, and f of Figure 1 show the representative $I-V$ curves collected in three Pt/10 nm TiO_{2-x}/Ti memristors, in which the TiO_{2-x} films were anodized at V_A = 2.5 V using 0.5 M H_3PO_4, 0.5 M NaOH, and 0.5 M $NH_4H_2PO_4$ electrolytes, respectively. The ramped voltage stresses (RVS) were applied to the Ti electrode, keeping the Pt one grounded. It is worth mentioning that, before the cyclical RS observed in parts d, e, and f of Figures 1, these devices exhibited typical forming processes observed for anodic RS devices,[35,36] with an initial dielectric breakdown voltage of 1.8, 1.4, and 2 V, respectively (see Supplementary Figure S4, SI). The statistical analysis of forming voltages is shown in Supplementary Figure S5 (SI), and we observed that the memristive devices fabricated using phosphate electrolytes (H_3PO_4, $NH_4H_2PO_4$) show smaller variations in forming voltages, possibly suggesting that more amorphous TiO_{2-x} films are formed using phosphate electrolytes. This is probably due to the phosphorus incorporation into the anodic oxide layer, thus inhibiting the crystallization of the anodic TiO_{2-x} film.[37−39] Figure 1d−f also shows that the cycle-to-cycle variability is very low and that the use of different electrolytes to grow the oxides does not remarkably affect the electrical characteristics of the devices; i.e., the electrochemical anodization method is not very sensitive to the species introduced in the electrolyte (at least for the concentrations and voltages used in this study). This is of particular relevance for the possible industrial transfer of this technology; indeed, given the independence of results obtained on the electrolyte composition, it is possible to select the anodizing electrolyte based on optimization parameters typical of the anodic process, i.e., reducing the aggressiveness of the electrolyte (to avoid risks for operators) and increasing

DOI: 10.1021/acs.chemmater.9b02245
Chem. Mater. 2019, 31, 8394−8401

repeatability, which strongly depends on the electrolyte composition.[26]

As shown in Figure 2a, the Pt/anodic TiO_{2-x}/Ti memristive devices show stable bipolar RS after forming; the set voltages (V_{SET}) are below 1 V, the reset processes can be progressively induced from −0.5 to −1.6 V, and the cycle-to-cycle variability during >4500 cycles is as low as that of other TMO-based memristors fabricated via ALD and sputtering.[14,32] This can be better observed from the resistance vs cycle plot (Figure 2b). It should be highlighted that the reset process in all anodic memristive devices is very progressive and stable; i.e., the resistance of the Pt/10 nm TiO_{2-x}/Ti memristors can be switched at different levels by stopping the reset ramp at different values (see Figure 2c and Supplementary Figure S6, SI), indicating that the RS in the Pt/anodic TiO_{2-x}/Ti memristors is a distributed effect, which is probably due to the large density of defects in the anodic TiO_{2-x} films. The high density of defects in the TiO_{2-x} film may allow charge transport by hopping and/or trap-assisted tunneling (TAT). This observation suggests that the RS behavior is modulated by electrical-field-driven ionic motion, although thermal effects related to the high currents flowing across the anodic oxide should not be discarded.[40,41] It is also observed that V_{SET} and V_{RESET} are stable at high temperatures up to 120 °C (Figure 2d), which may be useful to maintain the performance of the devices during prolonged operation times. By analyzing devices with different sizes down to 10 μm × 10 μm, it can be concluded that smaller anodic memristive devices show higher initial resistance (see Figure 2e) and that V_{SET} values becomes higher (Figure 2f), suggesting that larger devices may contain higher amounts of native defects in the TiO_{2-x} film, facilitating the generation of new defects under electrical field. The variability of V_{SET} within each device is remarkably small.

The switching time of anodic memristive devices (namely, t_{SET} and t_{RESET}) have been measured by applying alternating current (ac) fast pulse measurement. Figure 3 demonstrates that the devices can be set to LRS in as fast as 90 ns by applying a 1.5 V/2 μs SET pulse; the I_{LRS}/I_{HRS} ratio is >100 (see also Supplementary Figure S7, SI), and it can be reset within 130 ns under −2 V/2 μs RESET pulse. The pulse reset process shows abrupt current changes compared to the progressive RVS reset process, which is attributed to the high pulse amplitude applied in order to switch the device back to a high resistive state. The switching times are comparable to that of other memristors fabricated via ALD and sputtering.[42,43]

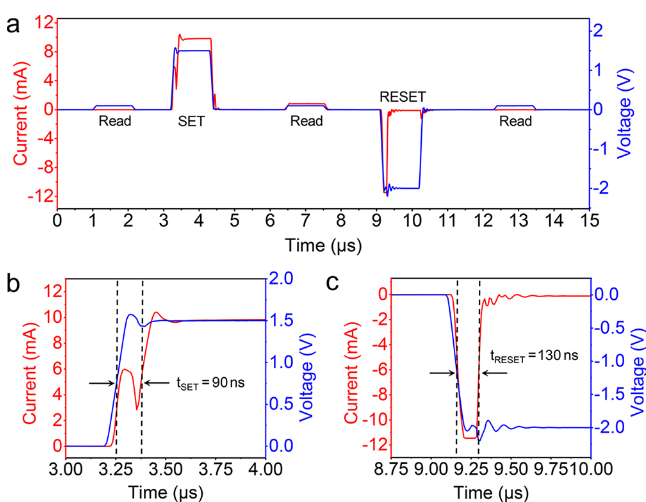

Figure 3. Fast interstate switching of anodic memristive synapses. (a) Pulse programming sequence of a Pt/10 nm TiO_{2-x}/Ti memristive device; the initial resistance is measured by a 0.1 V/1 μs pulse, followed by a 1.5 V/1 μs set pulse, a 0.1 V/1 μs read pulse, a −2 V/1 μs reset pulse, and another 0.1 V/1 μs read pulse. The switching times are shorter than 90 and 130 ns for set (b) and reset (c) processes.

To better understand the origin of the RS mechanism, the anodic memristive devices have been analyzed by cross-sectional transmission electron microscopy. Figure 3a,b shows the TEM images of a fresh Pt/anodic TiO_{2-x}/Ti (7.5 V, H_3PO_4) device, and the MIM memristor structure can be clearly identified. As can be observed, the morphology and thickness of anodic TiO_{2-x} films are very homogeneous (see Figure 4a−4c), which is in agreement with the CAFM analysis.

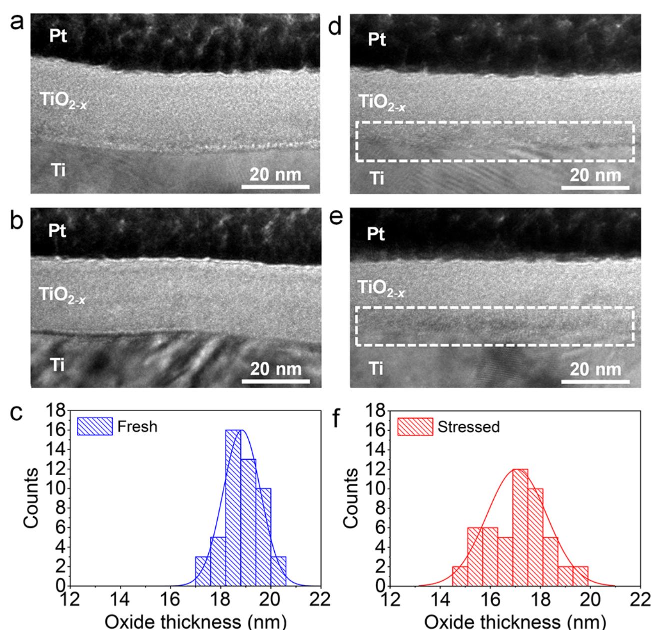

Figure 4. Morphological characterization of anodic memristive synapses. (a, b) Cross-sectional transmission electron microscopy images of a fresh anodic Pt/TiO_{2-x}/Ti memristive device (7.5 V, H_3PO_4) showing that the thickness and morphology of TiO_{2-x} grown by anodic oxidation are very homogeneous. The interfaces between each layer can be clearly identified. (c) Statistical distribution of TiO_{2-x} thickness in fresh devices. (d, e) TEM images of Pt/TiO_{2-x}/Ti memristive device after RVS and PVS tests (see Figure 5b−d). In comparison with the fresh regions, it can be observed that the morphology between TiO_{2-x} and Ti layers has been changed (indicated within white dashed areas), suggesting the generation of an interface layer between the TiO_{2-x} and Ti due to interfacial interactions under external electrical stimuli. The thickness of the interface layer is around 1−3 nm. (f) Statistical distribution of TiO_{2-x} thickness after RVS and PVS tests showing that TiO_{2-x} becomes thinner after applying electrical stress.

After the electrical RVS and pulsed voltage stress (PVS) characterization (see Figure 5b−d), we observed (in Figure 4d,e) that the bulk structure of the TiO_{2-x} film is still homogeneous and that the Pt/TiO_{2-x} interface remains unaltered. However, the morphology of the interface between the TiO_{2-x} and Ti layers experiences important changes (as highlighted within white dashed areas in Figure 4d,e; see more images in Supplementary Figure S8, SI), becoming less sharp

DOI: 10.1021/acs.chemmater.9b02245
Chem. Mater. 2019, 31, 8394−8401

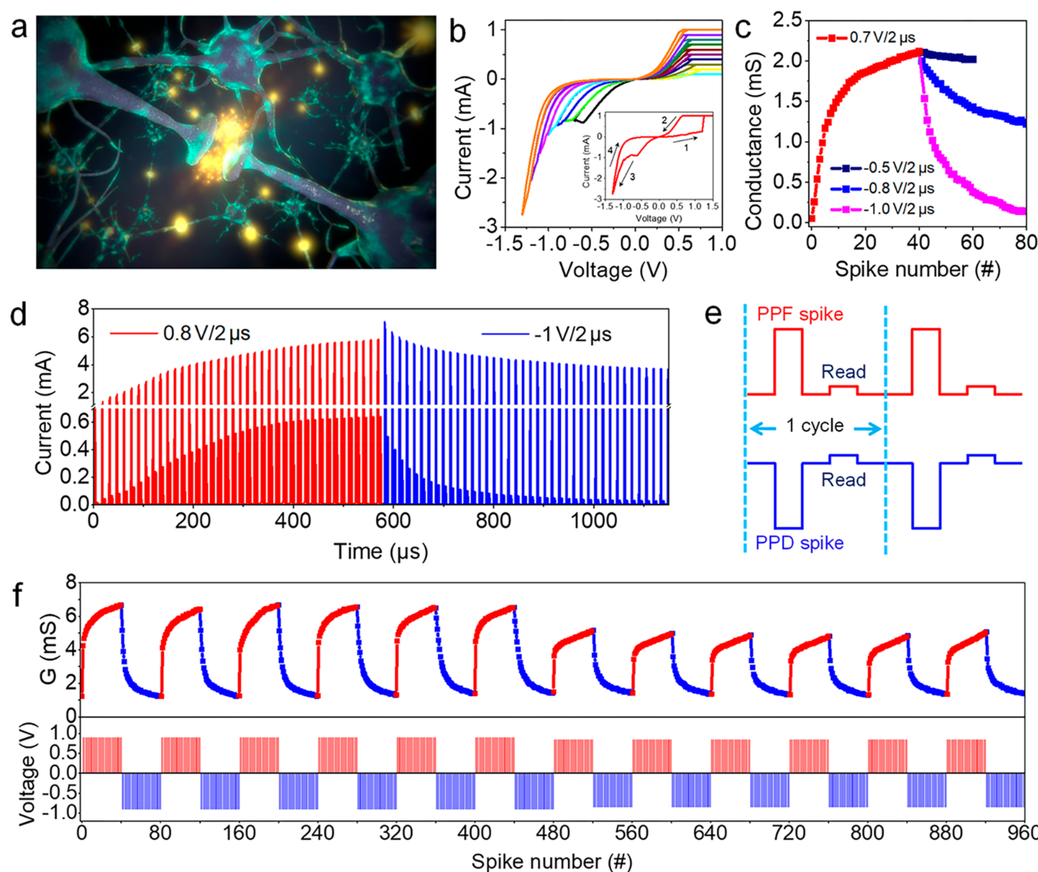

Figure 5. Synaptic behaviors of anodic memristive synapses. (a) Illustration of a biological neural network. (b) $I-V$ characteristics of a Pt/10 nm TiO_{2-x}/Ti memristive synapse (V_A = 2.5 V, NaOH), which shows progressive set (potentiation) and reset (depression) processes. The inset shows one switching cycle using 1 mA current compliance; the device shows a sudden increase of current during the set process, and during reset the conductance decreases very gradually. (c) Conductance change of the synapse under different programming pulses; the conductance was read by a 0.1 V/2 μs read pulse. (d) Paired-pulse facilitation and paired-pulse depression of an anodized memristive synapse by applying programming pulses of 40 PVS of 0.7 V/2 μs and 40 PVS of −1 V/2 μs, respectively. Each potentiation/depression spike was followed by a −0.1 V/2 μs read pulse. (e) The pulse waveform applied in parts c and d. (f) Potentiating (red) and depressing (blue) characteristics of anodic TiO_{2-x} synapse under consecutive programming pulses: 0.9 V/2 μs and −0.9 V/2 μs from spike 1 to 480, and 0.85 V/2 μs and −0.85 V/2 μs from spike 481 to 960. The conductance is read by a 0.1 V/2 μs pulse after each programming pulse.

and generating a dark interfacial layer with a thickness of ∼2 nm. This observation indicates the phase change of the TiO_{2-x} film, probably due to the crystallization of TiO_{2-x} under high joule heating temperatures during the electroforming and RVS and PVS measurements.[44−47] This tiny interface film has been also analyzed via energy dispersive X-ray spectroscopy (EDX) and electron energy loss spectroscopy (EELS) integrated in the TEM system; however, the small thickness of this film impeded reliable detection of its chemical composition. Nevertheless, from the TEM images it is very clear that the thickness of the TiO_{2-x} reduces ∼2 nm after the stress, as statistically corroborated in Figure 4f, which is very similar to the thickness of the dark layer at the TiO_{2-x}/Ti interface. As the initial stress has been induced by applying positive bias to the bottom Ti electrode, it is reasonable to assume that O^{2-} ions migrate toward it, reducing the thickness of the TiO_{2-x} film. This observation indicates that the resistive switching of the Pt/anodic TiO_{2-x}/Ti memristive synapse takes place at the interface oxide layer that generated between the Ti electrode and the titanium oxide. The reversible resistive switching between HRS and LRS is attributed to the reversible oxidation and reduction of the interfacial oxide layer. This interfacial RS mechanism is consistent with previous reports in the field of RS-based NVMs,[48,49] but so far it has never been pplied to the fabrication of electronic synapses made of anodized TMO films.

In the next step, the temporal response and synaptic capabilities of the Pt/anodic TiO_{2-x}/Ti memristors were analyzed. Figure 5a shows the schematic of a biological neural network, highlighting the charge exchange process at the synapses. The synapses are connections between presynaptic neurons and postsynaptic neurons, and by changing their strength, e.g., synaptic weight (ω) or conductance (G), synapses can contribute to transmit the input signal from presynaptic neurons to postsynaptic neurons.[8] Here, the analog synaptic plasticity, i.e., the ability to continuously adjust the conductance of the anodic memristive synapse, could be implemented by varying the current compliance in the dc set process and incremental reset sweeps during dc programming. As shown in Figure 5b, 10 different conductance states can be readily achieved using different current compliances ranging from 100 μA to 1 mA, and the devices could be gradually reset by applying consecutive sweeps from −0.7 to −1.3 V with a step of 100 mV. The achievement of multilevel conductance states of anodic TiO_{2-x} memristive devices is consistent with previous memristive devices fabricated using ALD-grown

DOI: 10.1021/acs.chemmater.9b02245
Chem. Mater. 2019, 31, 8394−8401

HfO_x/AlO_x and TiO_{2-x} as dielectric layers.[3,50] More importantly, the implementation of gradual conductance changes has been also achieved by applying sequences of ac training pulses. By varying the pulse amplitude, long-term depression of the anodic synapses could be accurately controlled (Figure 5c), which is consistent with the observation of gradual conductance change under different dc reset voltages. It is found that, under higher programing amplitudes, the memristive synapse exhibits faster conductance change, and smaller programing amplitudes lead to a slower conductance change. Figure 5d shows the paired-pulse facilitation (PPF) and paired-pulse depression (PPD) of a $Pt/TiO_{2-x}/Ti$ memristive synapse programmed by 40 consecutive identical positive pulses (0.7 V/2 μs) followed by 40 consecutive identical negative pulses (−1 V/2 μs). In this measurement, each programming pulse was followed by a nondisturbing read pulse (0.1 V/2 μs), as shown in Figure 5e. The gradual increase and decrease of current in Figure 5d demonstrate the capability of anodic synapses to emulate synaptic long-term potentiation and depression behavior.[4] Furthermore, the devices exhibit stable potentiation and depression characteristics during more than 960 programming pulses (see Figure 5f). In Figure 5f, it is also demonstrated that the conductance can be tuned by the amplitude of the pulses applied; i.e., the first six cycles (from spike 0 to 480) used pulses of ±0.9 V and produced G_{MAX} of 7 mS, while the last six cycles (from spike 481 to 960) used pulses of ±0.85 V and produced a G_{MAX} of 5 mS. These observations demonstrate that TiO_{2-x} films prepared by the anodic oxidation method are excellent RS media for the fabrication of memristive synapses, allowing multilevel conductance states under both dc and ac electrical impulses with short (<90 ns) interstate switching and showing synapse-like potentiating and depressing characteristics.

■ CONCLUSION

In summary, we have fabricated the first memristive synapses using a transition-metal oxide (TiO_{2-x}) synthesized by anodic oxidation. Pt/anodic TiO_{2-x}/Ti memristors show bipolar resistive switching with low programming voltages, low variability, and multistate conductance under different current compliance and reset voltages, as well as fast switching times down to 90 ns. The switching mechanism is governed by interface charge rearrangements and TiO_{2-x} thickness modulation via bipolar electrical impulses. We successfully tuned the conductance of the anodized synapses very gradually by applying sequences of pulsed voltage stresses, and the speed for potentiation and depression could be adjusted by changing the pulse amplitude. It is concluded that anodization shows strong potential for the fabrication of memristive electronic synapses, which could have important implications for the development of neuromorphic computational systems.

■ METHODS

Estimation of Oxide Thickness. At low anodization voltages, the thickness of the TiO_{2-x} films is derived from the total charge supplied,[26] so it can be calculated with Faraday's law[51,52]

$$Q = i\Delta t = zF\rho A\varphi/M \quad (4)$$

where Q is the total charge in the anodization system, i the current density, Δt is the anodizing time, z is the valence of titanium ions (+4), F is Faraday's constant (96 485 C/mol), ρ is the density of titanium oxide, A is the anodized area, φ is the anodized oxide thickness, and M is the molecular weight of TiO_{2-x}. At voltages where relevant parasitic processes occur (mainly oxygen evolution), subtracting current to the oxide growth, this method is not reliable anymore.[53] If the oxide is thick enough to produce interference colors (on the order of 40 nm, generally achieved at $V_A > 10$ V), then it is possible to estimate oxide thickness from the position of interference maxima (eq 5) and minima (eq 6), as follows

$$d = nm\lambda/2 \quad (5)$$

$$d = n(2m + 1)\lambda/4 \quad (6)$$

where d is the film thickness, n is the oxide refractive index, m is the order of interference, and λ is the wavelength at which the maximum or minimum in the reflectance spectrum was identified.[22,25] The details have been exhaustively described in ref 54.

Memristive Synapse Fabrication. The $Pt/TiO_{2-x}/Ti$ memristive devices have been fabricated by evaporating 50 nm Pt as top electrodes on the anodic TiO_{2-x}/Ti samples. The electrodes were deposited using an electron beam evaporator system from Kurt J. Lesker (model PVD 75) and a laser-patterned shadow mask; the size of the top electrodes ranged from 10 μm × 10 μm to 100 μm × 100 μm.

Conductive Atomic Force Microscope Charcterization. The morphology and electrical properties of anodic TiO_{2-x} were characterized using an atomic force microscope from Bruker (model Dimension Icon) working in ambient atmosphere. The topographic and current maps, as well as the current vs voltage (I−V) curves, have been collected in contact mode using Pt−Ir-coated silicon probes (tip radius <25 nm) from Nanosensors (Model PPP-CONTPt-50). The bias (ramped from 0 V to negative voltages) was always applied to the sample, keeping the tip grounded.

Synapse Electrical Characterization. Current vs voltage (I−V) characteristics of the memristive synapses have been measured by applying ramped voltage stresses (RVS) using two different semiconductor parameter analyzers (SPA), one Keithley 4200-SCS and one Keysight B1500A, working in ambient conditions. Current-visible pulsed voltage stresses (PVS)—in which the current vs time is monitored during the PVS—as fast as 10 ns have been applied using a Keysight B1530A waveform generator fast measurement unit (WGFMU), connected to the Keysight B1500A SPA. In all synapses, the RVS and PVS were applied to the bottom Ti electrodes, while the top Pt electrodes were grounded.

Optical Microscope Characterization. The surface of the TiO_{2-x} films in Figure 1b were analyzed using a fluorescence optical microscope from Leica Microsystems (model DMi8).

Transmission Electron Microscope Characterization. The fresh (as fabricated) and stressed $Pt/TiO_{2-x}/Ti$ memristive synapses (the RVS and PVS tests can be seen in Figure 5b,f) were first cut by a focus ion beam (FIB), which is integrated in a FEI FEI-Scios 2 Hivac scanning electron microscope (SEM) system. The resolution of the ion beam was below 3 nm. Then, the thin lamellas were placed on a copper grid and inspected using Tecnai G2 F20 S-Twin and JEOL JEM-2100 transmission electron microscope, equipped with electron dispersive X-ray spectroscopy (EDX) and electron energy loss spectroscopy (EELS). The EDS and EELS analyses were carried out during high-angle annular dark-field scanning transmission electron microscopy (HAADF-STEM).

■ ASSOCIATED CONTENT

Supporting Information

The Supporting Information is available free of charge on the ACS Publications website at DOI: 10.1021/acs.chemmater.9b02245.

CAFM analysis of anodic TiO_{2-x} films, statistic distribution of the onset potential, dc forming and reset characteristics, pulse set and reset data, and TEM characterization (PDF)

DOI: 10.1021/acs.chemmater.9b02245
Chem. Mater. 2019, 31, 8394−8401

■ AUTHOR INFORMATION

Corresponding Author

*E-mail: mlanza@suda.edu.cn.

ORCID

Mario Lanza: 0000-0003-4756-8632

Author Contributions

M.L., M.V.D., MP.P., S.N., and S.C conceived the initial concept and designed the experiments; S.N. and M.V.D. grew the TiO_{2-x} films; S.C. fabricated memristive synapses; S.C., S.N., Y.S., and M.L. developed the measurement setup. S.C., Y.S., T.H., and Y.Z performed the experiment; M.A.V assisted on data analysis; M.L., M.V.D., and D.S. supervised this project; S.C. and M.L. wrote the manuscript. All authors discussed the data and results.

Notes

The authors declare no competing financial interest.

■ ACKNOWLEDGMENTS

This work has been supported by the Young 1000 Global Talent Recruitment Program of the Ministry of Education of China, the Ministry of Science and Technology of China (grant no. BRICS2018-211-2DNEURO), the National Natural Science Foundation of China (grants no. 61502326, 41550110223, 11661131002, 61874075), the Ministry of Finance of China (grant no. SX21400213), and the Young 973 National Program of the Chinese Ministry of Science and Technology (grant no. 2015CB932700). The Collaborative Innovation Center of Suzhou Nano Science & Technology, the Jiangsu Key Laboratory for Carbon-Based Functional Materials & Devices, the Priority Academic Program Development of Jiangsu Higher Education Institutions, and the 111 Project from the State Administration of Foreign Experts Affairs are also acknowledged. S.N., MP.P., and M.V.D. acknowledge the financial support of Fondazione Cariplo and Regione Lombardia, project ProACTIV-MOX—PROmoting research on AnodiC memris TIVe Metal OXide films for nano-electronics.

■ REFERENCES

(1) Hasler, J.; Marr, B. Finding a Roadmap to Achieve Large Neuromorphic Hardware Systems. *Front. Neurosci.* **2013**, *7*, 118.

(2) Kuzum, D.; Jeyasingh, R. G. D.; Lee, B.; Wong, H.-S. P. Nanoelectronic Programmable Synapses Based on Phase Change Materials for Brain-Inspired Computing. *Nano Lett.* **2012**, *12*, 2179−2186.

(3) Yu, S.; Wu, Y.; Jeyasingh, R.; Kuzum, D.; Wong, H.-S. P. An Electronic Synapse Device Based on Metal Oxide Resistive Switching Memory for Neuromorphic Computation. *IEEE Trans. Electron Devices* **2011**, *58*, 2729−2737.

(4) Ambrogio, S.; Narayanan, P.; Tsai, H.; Shelby, R. M.; Boybat, I.; Di Nolfo, C.; Sidler, S.; Giordano, M.; Bodini, M.; Farinha, N. C. P.; Killeen, B.; Cheng, C.; Jaoudi, Y.; Burr, G. W. Equivalent-Accuracy Accelerated Neural-Network Training Using Analogue Memory. *Nature* **2018**, *558*, 60−67.

(5) Prezioso, M.; Merrikh-Bayat, F.; Hoskins, B. D.; Adam, G. C.; Likharev, K. K.; Strukov, D. B. Training and Operation of an Integrated Neuromorphic Network Based on Metal-Oxide Memristors. *Nature* **2015**, *521*, 61−64.

(6) Bayat, F. M.; Prezioso, M.; Chakrabarti, B.; Nili, H.; Kataeva, I.; Strukov, D. Implementation of Multilayer Perceptron Network with Highly Uniform Passive Memristive Crossbar Circuits. *Nat. Commun.* **2018**, *9*, 2331.

(7) Kuzum, D.; Yu, S.; Wong, H.-S. P. Synaptic Electronics: Materials, Devices and Applications. *Nanotechnology* **2013**, *24*, 382001.

(8) Boyn, S.; Grollier, J.; Lecerf, G.; Xu, B.; Locatelli, N.; Fusil, S.; Girod, S.; Carrétéro, C.; Garcia, K.; Xavier, S.; Tomas, J.; Bellaiche, L.; Bibes, M.; Barthélémy, A.; Saïghi, S.; Garcia, V. Learning through Ferroelectric Domain Dynamics in Solid-State Synapses. *Nat. Commun.* **2017**, *8*, 14736.

(9) Merolla, P. A.; Arthur, J. V.; Alvarez-Icaza, R.; Cassidy, A. S.; Sawada, J.; Akopyan, F.; Jackson, B. L.; Imam, N.; Guo, C.; Nakamura, Y.; Brezzo, B.; Vo, I.; Esser, S. K.; Appuswamy, R.; Taba, B.; Amir, A.; Flickner, M. D.; Risk, W. P.; Manohar, R.; Modha, D. S. A Million Spiking-Neuron Integrated Circuit with a Scalable Communication Network and Interface. *Science* **2014**, *345*, 668−673.

(10) Yang, J. J.; Strukov, D. B.; Stewart, D. R. Memristive Devices for Computing. *Nat. Nanotechnol.* **2013**, *8*, 13−24.

(11) van de Burgt, Y.; Melianas, A.; Keene, S. T.; Malliaras, G.; Salleo, A. Organic Electronics for Neuromorphic Computing. *Nat. Electron.* **2018**, *1*, 386−397.

(12) Ohno, T.; Hasegawa, T.; Tsuruoka, T.; Terabe, K.; Gimzewski, J. K.; Aono, M. Short-Term Plasticity and Long-Term Potentiation Mimicked in Single Inorganic Synapses. *Nat. Mater.* **2011**, *10*, 591−595.

(13) Shi, Y.; Pan, C.; Chen, V.; Raghavan, N.; Pey, K. L.; Puglisi, F. M.; Pop, E.; Wong, H.-S. P.; Lanza, M. Coexistence of Volatile and Non-Volatile Resistive Switching in 2D h-BN Based Electronic Synapses. In *2017 IEEE International Electron Devices Meeting (IEDM)*; IEEE, 2017; pp 5.4.1−5.4.4.

(14) Shi, Y.; Liang, X.; Yuan, B.; Chen, V.; Li, H.; Hui, F.; Yu, Z.; Yuan, F.; Pop, E.; Wong, H.-S. P.; Lanza, M. Electronic Synapses Made of Layered Two-Dimensional Materials. *Nat. Electron.* **2018**, *1*, 458−465.

(15) Brenna, A.; Corinto, F.; Noori, S.; Ormellese, M.; Pedeferri, M.; Diamanti, M. V. Memristive Anodic Oxides: Production, Properties and Applications in Neuromorphic Computing. In *Advances in Memristor Neural Networks—Modeling and Applications*; Ciufudean, C., Ed.; InTech, 2018.

(16) Ielmini, D.; Waser, R. *Resistive Switching: From Fundamentals of Nanoionic Redox Processes to Memristive Device Applications*; Wiley-VCH: Weinheim, Germany, 2016.

(17) Hui, F.; Grustan-Gutierrez, E.; Long, S.; Liu, Q.; Ott, A. K.; Ferrari, A. C.; Lanza, M. Graphene and Related Materials for Resistive Random Access Memories. *Adv. Electron. Mater.* **2017**, *3*, 1600195.

(18) Pan, C.; Ji, Y.; Xiao, N.; Hui, F.; Tang, K.; Guo, Y.; Xie, X.; Puglisi, F. M.; Larcher, L.; Miranda, E.; Jiang, L.; Shi, Y.; Valov, I.; McIntyre, P. C.; Waser, R.; Lanza, M. Coexistence of Grain-Boundaries-Assisted Bipolar and Threshold Resistive Switching in Multilayer Hexagonal Boron Nitride. *Adv. Funct. Mater.* **2017**, *27*, 1604811.

(19) Valov, I.; Waser, R.; Jameson, J. R.; Kozicki, M. N. Electrochemical Metallization Memories—Fundamentals, Applications, Prospects. *Nanotechnology* **2011**, *22*, 254003.

(20) Sawa, A. Resistive Switching in Transition Metal Oxides. *Mater. Today* **2008**, *11*, 28−36.

(21) van de Burgt, Y.; Lubberman, E.; Fuller, E. J.; Keene, S. T.; Faria, G. C.; Agarwal, S.; Marinella, M. J.; Alec Talin, A.; Salleo, A. A Non-Volatile Organic Electrochemical Device as a Low-Voltage Artificial Synapse for Neuromorphic Computing. *Nat. Mater.* **2017**, *16*, 414−418.

(22) Sul, Y.-T.; Johansson, C. B.; Jeong, Y.; Albrektsson, T. The Electrochemical Oxide Growth Behaviour on Titanium in Acid and Alkaline Electrolytes. *Med. Eng. Phys.* **2001**, *23*, 329−346.

(23) Zaffora, A.; Cho, D.-Y.; Lee, K.-S.; Di Quarto, F.; Waser, R.; Santamaria, M.; Valov, I. Electrochemical Tantalum Oxide for Resistive Switching Memories. *Adv. Mater.* **2017**, *29*, 1703357.

(24) Aglieri, V.; Zaffora, A.; Lullo, G.; Santamaria, M.; Di Franco, F.; Lo Cicero, U.; Mosca, M.; Macaluso, R. Resistive Switching in Microscale Anodic Titanium Dioxide-Based Memristors. *Superlattices Microstruct.* **2018**, *113*, 135−142.

DOI: 10.1021/acs.chemmater.9b02245
Chem. Mater. 2019, 31, 8394−8401

(25) Diamanti, M. V.; Ormellese, M.; Pedeferri, M. Application-Wise Nanostructuring of Anodic Films on Titanium: A Review. *J. Exp. Nanosci.* **2015**, *10*, 1285−1308.
(26) Diamanti, M. V.; Pozzi, P.; Randone, F.; Del Curto, B.; Pedeferri, M. Robust Anodic Colouring of Titanium: Effect of Electrolyte and Colour Durability. *Mater. Des.* **2016**, *90*, 1085−1091.
(27) Habazaki, H.; Uozumi, M.; Konno, H.; Shimizu, K.; Skeldon, P.; Thompson, G. E. Crystallization of Anodic Titania on Titanium and Its Alloys. *Corros. Sci.* **2003**, *45* (9), 2063−2073.
(28) Xiao, N.; Villena, M. A.; Yuan, B.; Chen, S.; Wang, B.; Eliáš, M.; Shi, Y.; Hui, F.; Jing, X.; Scheuermann, A.; Tang, K.; McIntyre, P. C.; Lanza, M. Resistive Random Access Memory Cells with a Bilayer TiO_2/SiO_x Insulating Stack for Simultaneous Filamentary and Distributed Resistive Switching. *Adv. Funct. Mater.* **2017**, *27* (33), 1700384.
(29) Lee, M.-J.; Lee, C. B.; Lee, D.; Lee, S. R.; Chang, M.; Hur, J. H.; Kim, Y.-B.; Kim, C.-J.; Seo, D. H.; Seo, S.; Chung, U.-I.; Yoo, I.-K.; Kim, K. A Fast, High-Endurance and Scalable Non-Volatile Memory Device Made from Asymmetric Ta_2O_{5-x}/TaO_{2-x} Bilayer Structures. *Nat. Mater.* **2011**, *10*, 625−630.
(30) Ji, Y.; Pan, C.; Zhang, M.; Long, S.; Lian, X.; Miao, F.; Hui, F.; Shi, Y.; Larcher, L.; Wu, E.; Lanza, M. Boron Nitride as Two Dimensional Dielectric: Reliability and Dielectric Breakdown. *Appl. Phys. Lett.* **2016**, *108*, 012905.
(31) Bayerl, A.; Lanza, M.; Porti, M.; Nafria, M.; Aymerich, X.; Campabadal, F.; Benstetter, G. Nanoscale and Device Level Gate Conduction Variability of High-k Dielectrics-Based Metal-Oxide-Semiconductor Structures. *IEEE Trans. Device Mater. Reliab.* **2011**, *11*, 495−501.
(32) Lanza, M.; Wong, H.-S. P.; Pop, E.; Ielmini, D.; Strukov, D.; Regan, B. C.; Larcher, L.; Villena, M. A.; Yang, J. J.; Goux, L.; Belmonte, A.; Yang, Y.; Puglisi, F. M.; Kang, J.; Magyari-Köpe, B.; Yalon, E.; Kenyon, A.; Buckwell, M.; Mehonic, A.; Shluger, A.; Li, H.; Hou, T.-H.; Hudec, B.; Akinwande, D.; Ge, R.; Ambrogio, S.; Roldan, J. B.; Miranda, E.; Suñe, J.; Pey, K. L.; Wu, X.; Raghavan, N.; Wu, E.; Lu, W. D.; Navarro, G.; Zhang, W.; Wu, H.; Li, R.; Holleitner, A.; Wurstbauer, U.; Lemme, M. C.; Liu, M.; Long, S.; Liu, Q.; Lv, H.; Padovani, A.; Pavan, P.; Valov, I.; Jing, X.; Han, T.; Zhu, K.; Chen, S.; Hui, F.; Shi, Y. Recommended Methods To Study Resistive Switching Devices. *Adv. Electron. Mater.* **2019**, *5*, 1800143.
(33) Wang, S.; Chen, C.; Yu, Z.; He, Y.; Chen, X.; Wan, Q.; Shi, Y.; Zhang, D. W.; Zhou, H.; Wang, X.; Zhou, P. A MoS_2/PTCDA Hybrid Heterojunction Synapse with Efficient Photoelectric Dual Modulation and Versatility. *Adv. Mater.* **2019**, *31*, 1806227.
(34) Zhong, Y.-N.; Wang, T.; Gao, X.; Xu, J.-L.; Wang, S.-D. Synapse-Like Organic Thin Film Memristors. *Adv. Funct. Mater.* **2018**, *28*, 1800854.
(35) Zaffora, A.; Di Quarto, F.; Habazaki, H.; Valov, I.; Santamaria, M. Electrochemically Prepared Oxides for Resistive Switching Memories. *Faraday Discuss.* **2019**, *213*, 165−181.
(36) Zaffora, A.; Macaluso, R.; Habazaki, H.; Valov, I.; Santamaria, M. Electrochemically Prepared Oxides for Resistive Switching Devices. *Electrochim. Acta* **2018**, *274*, 103−111.
(37) Afshar, A.; Vaezi, M. R. Evaluation of Electrical Breakdown of Anodic Films on Titanium in Phosphate-Base Solutions. *Surf. Coat. Technol.* **2004**, *186* (3), 398−404.
(38) Ferdjani, S.; David, D.; Beranger, G. Anodic Oxidation of Titanium in Phosphoric Acid Baths: Phosphorus Incorporation into the Oxide. *J. Alloys Compd.* **1993**, *200* (1−2), 191−194.
(39) Ohtsu, N.; Ishikawa, D.; Komiya, S.; Sakamoto, K. Effect of Phosphorous Incorporation on Crystallinity, Morphology, and Photocatalytic Activity of Anodic Oxide Layer on Titanium. *Thin Solid Films* **2014**, *556*, 247−252.
(40) Borghetti, J.; Strukov, D. B.; Pickett, M. D.; Yang, J. J.; Stewart, D. R.; Williams, R. S. Electrical Transport and Thermometry of Electroformed Titanium Dioxide Memristive Switches. *J. Appl. Phys.* **2009**, *106*, 124504.
(41) Strukov, D. B.; Williams, R. S. Intrinsic Constrains on Thermally-Assisted Memristive Switching. *Appl. Phys. A: Mater. Sci. Process.* **2011**, *102*, 851−855.
(42) Wang, Z.; Yin, M.; Zhang, T.; Cai, Y.; Wang, Y.; Yang, Y.; Huang, R. Engineering incremental resistive switching in TaO_x based memristors for brain-inspired computing. *Nanoscale* **2016**, *8*, 14015−14022.
(43) Kim, H.; Kim, H.; Hwang, S.; Kim, M.-H.; Chang, Y.-F.; Park, B.-G. Analog Synaptic Behavior of a Silicon Nitride Memristor. *ACS Appl. Mater. Interfaces* **2017**, *9*, 40420−40427.
(44) Münstermann, R.; Yang, J. J.; Strachan, J. P.; Medeiros-Ribeiro, G.; Dittmann, R.; Waser, R. Morphological and Electrical Changes in TiO_2 Memristive Devices Induced by Electroforming and Switching. *Phys. Status Solidi RRL* **2010**, *4* (1−2), 16−18.
(45) Strukov, D. B.; Borghetti, J. L.; Williams, R. S. Coupled Ionic and Electronic Transport Model of Thin-Film Semiconductor Memristive Behavior. *Small* **2009**, *5* (9), 1058−1063.
(46) Strachan, J. P.; Joshua Yang, J.; Münstermann, R.; Scholl, A.; Medeiros-Ribeiro, G.; Stewart, D. R.; Stanley Williams, R. Structural and Chemical Characterization of TiO_2 Memristive Devices by Spatially-Resolved NEXAFS. *Nanotechnology* **2009**, *20* (48), 485701.
(47) Strachan, J. P.; Pickett, M. D.; Yang, J. J.; Aloni, S.; David Kilcoyne, A. L.; Medeiros-Ribeiro, G.; Stanley Williams, R. Direct Identification of the Conducting Channels in a Functioning Memristive Device. *Adv. Mater.* **2010**, *22* (32), 3573−3577.
(48) Valov, I. Interfacial Interactions and Their Impact on Redox-Based Resistive Switching Memories (ReRAMs). *Semicond. Sci. Technol.* **2017**, *32*, 093006.
(49) Lübben, M.; Karakolis, P.; Ioannou-Sougleridis, V.; Normand, P.; Dimitrakis, P.; Valov, I. Graphene-Modified Interface Controls Transition from VCM to ECM Switching Modes in Ta/TaO_x Based Memristive Devices. *Adv. Mater.* **2015**, *27*, 6202−6207.
(50) Alibart, F.; Gao, L.; Hoskins, B. D.; Strukov, D. B. High Precision Tuning of State for Memristive Devices by Adaptable Variation-Tolerant Algorithm. *Nanotechnology* **2012**, *23* (7), 075201.
(51) Schroth, S.; Schneider, M.; Mayer-Uhma, T.; Michaelis, A.; Klemm, V. Investigation of thin oxide films on titanium for capacitor applications. *Surf. Interface Anal.* **2008**, *40*, 850−852.
(52) Diamanti, M. V.; Souier, T.; Stefancich, M.; Chiesa, M.; Pedeferri, M. P. Probing anodic oxidation kinetics and nanoscale heterogeneity within TiO_2 films by Conductive Atomic Force Microscopy and combined techniques. *Electrochim. Acta* **2014**, *129*, 203−210.
(53) Diamanti, M. V.; Spreafico, F. C.; Pedeferri, M. P. Production of Anodic TiO_2 Nanofilms and Their Characterization. *Phys. Procedia* **2013**, *40*, 30−37.
(54) Diamanti, M. V.; Del Curto, B.; Pedeferri, M. Interference Colors of Thin Oxide Layers on Titanium. *Color Res. Appl.* **2008**, *33* (3), 221−228.

DOI: 10.1021/acs.chemmater.9b02245
Chem. Mater. 2019, 31, 8394−8401